Iranian Journal of Numerical Analysis and Optimization
Vol. 16, No. 3, 2026, pp 1133–1160
https://doi.org/10.22067/ijnao.2026.96880.1797
https://ijnao.um.ac.ir/

Research Article

Quasilinearized Genocchi-Polynomial Collocation for Efficient Simulation of a Nonlinear SIRV Anthrax Transmission Model

N. Mohamed, M. El-Gamel and W. Adel*

Abstract

Mathematical models of anthrax transmission often involve strong nonlinearities that challenge standard solvers and can limit robust inference. We present a four-compartment (SIRV) animal anthrax model and an efficient numerical framework that combines quasilinearization with a shifted Genocchi-polynomial collocation scheme (Genocchi-QLM). We provide convergence and error analyses for the approximations on a finite interval and construct a residual-error diagnostic to certify solution quality. Across representative parameter sets, Genocchi-QLM achieves rapid convergence and close agreement with a benchmark Runge–Kutta implementation (`ode45`), while maintaining numerical stability over long horizons. We further

*Corresponding author

Received 7 December 2025; revised 21 April 2026; accepted 28 April 2026

Nesreen Mohamed
Department of Basic Science, Faculty of Engineering, Horus University, New Damietta 34517, Egypt. e-mail: nesreen.msedik@gmail.com

Mohamed El-Gamel
Department of Mathematics and Engineering Physics, Faculty of Engineering, Mansoura University, Mansoura 35516, Egypt. e-mail: gamel_eg@yahoo.com

Waleed Adel
Nanoelectronics Integrated Systems Center, Nile University, Giza, 12588, Egypt. Department of Mathematics and Engineering Physics, Faculty of Engineering, Mansoura University, Mansoura, 35516, Egypt. e-mail: waleed.ouf@ufe.edu.eg

How to cite this article
Mohamed, N., El-Gamel, M. and Adel, W., Quasilinearized Genocchi-Polynomial Collocation for Efficient Simulation of a Nonlinear SIRV Anthrax Transmission Model. *Iran. J. Numer. Anal. Optim.*, 2026; 16(3): 1133-1160. https://doi.org/10.22067/ijnao.2026.96880.1797

assess practical relevance by comparing simulated infected-case trajectories to reported outbreak patterns from endemic settings, observing qualitative agreement in rise-and-decay phases consistent with recovery, mortality, vaccination, and waning-immunity mechanisms. Sensitivity exploration highlights how vaccination rate and immunity waning jointly shape persistence. Because the method converts a nonlinear initial-value problem into a sequence of linear systems with a sparse structure, it is readily extensible to higher-dimensional or controlled models and can be adapted to fractional or stochastic variants. These results indicate that Genocchi-QLM is a fast, accurate, and scalable tool for solving nonlinear epidemiological systems and for supporting data-informed analysis of anthrax control strategies.

AMS subject classifications (2020): 92D30; 65L05; 65L07; 65M70; 42C10.

Keywords: Anthrax Disease Model; Boundary Value Problems; Genocchi Quasilinearization Method; Genocchi Polynomials; Numerical Methods.

1 Introduction

Bacillus anthracis is the bacterium that causes anthrax, an acute and often fatal zoonotic disease that has been recognized for centuries as a major threat to both animal and human health [25, 30]. Both domestic and wild animals are affected by the disease, with herbivorous species such as cattle, horses, sheep, goats, and antelopes being the most vulnerable due to their frequent contact with contaminated soil, water, or vegetation. These animals have very low natural resistance to anthrax, making it one of the most dangerous infectious diseases in the world [28, 36]. Bacillus anthracis bacterium is a spore-forming, rod-shaped organism that can survive in soil for decades under harsh environmental conditions; allowing repeated outbreaks in endemic regions. Infection in animals occurs in a variety of ways, such as by consuming water or grass contaminated with spores, inhaling spores while grazing, or coming into contact with carcasses of diseased animals [10].

Humans are also susceptible to anthrax and can contract the disease through direct or indirect contact with infected animals or their byproducts, including hides, wool, and meat [13]. Anthrax transmission occurs mainly through four well-recognized pathways [34]. Cutaneous anthrax enters the body through cuts or abrasions in the skin and is the most common form; although it is less deadly, untreated cases can still progress to systemic infection. Gastrointestinal anthrax develops after the ingestion of raw or undercooked meat from infected animals and is associated with severe abdominal pain, vomiting, and diarrhea, sometimes progressing rapidly to systemic illness. Pulmonary anthrax, also known as inhalation anthrax, results from breathing in

airborne spores and is the most dangerous form; even with treatment, it often has a high fatality rate due to rapid progression to severe respiratory distress and septicemia. Injection anthrax, the most recently identified form, occurs in people who inject contaminated drugs, leading to severe soft-tissue infections and sepsis.

Clinically, anthrax symptoms vary according to the route of infection but often share common features, including fever, fatigue, and rapid deterioration in severe cases. Cutaneous anthrax typically presents as a painless ulcer with a characteristic black eschar. Inhalation anthrax often begins with mild flu-like symptoms but quickly advances to respiratory failure if untreated. Gastrointestinal anthrax may cause severe hemorrhagic gastroenteritis, while injection anthrax is marked by extensive tissue damage and systemic toxicity. Globally, anthrax remains a significant public health and veterinary concern, particularly in Sub-Saharan Africa, parts of Asia, and some regions of North America where the bacteria are endemic in the soil. In recent decades, outbreaks in animal populations have been documented in several countries. In South Africa's Kruger National Park, for instance, the number of roan antelope plummeted from 450 to just 45 due to recurring anthrax outbreaks [11, 6]. In Tanzania, outbreaks have caused the deaths of 10 cattle, 26 goats, 3 sheep, and 131 wild animals, in addition to 21 humans suspected to the infection in a single season [22]. Human outbreaks have also been reported; in the Kilimanjaro region, 36 individuals were hospitalized after consuming anthrax-contaminated beef [26]. Tragically, in Arusha, eight of the 134 infected individuals succumbed to the disease, and in Dar es Salaam, six of the 22 infected patients died [26]. In Northern Canada, nine separate anthrax epidemics in bison populations were reported between 1962 and 1993, underscoring the persistent environmental reservoirs of the pathogen [7]. These examples highlight the enduring global presence of anthrax and the critical need for surveillance, rapid diagnosis, and effective vaccination programs to control its spread. Therefore, mathematical modeling plays a crucial role in predicting the spread of the disease and in understanding its complex dynamics, making it an essential tool for effective analysis and control strategies. The main modes of transmission of the anthrax in humans and animals can be seen in Figure 1.

Over the years, a number of mathematical models have been presented to explain how anthrax spreads among animals. Mushayabasa [24] created the first basic model of the dynamics of anthrax disease transmission, which included three main compartments: Pathogens, Contamination, and Susceptible. However, in this initial model, the role of infectious animals as a major contributor to the spread of anthrax was not addressed. Building on this foundation, Sabir and Simbawa [33] applied Bayesian regularization to develop a stochastic machine learning approach that demonstrated the numerical performance of the anthrax disease system in animal populations. In addition, Raza and Abdella [31] further examined the nonlinear dynamics of anthrax transmission by incorporating delay effects to account for the incubation period mech-

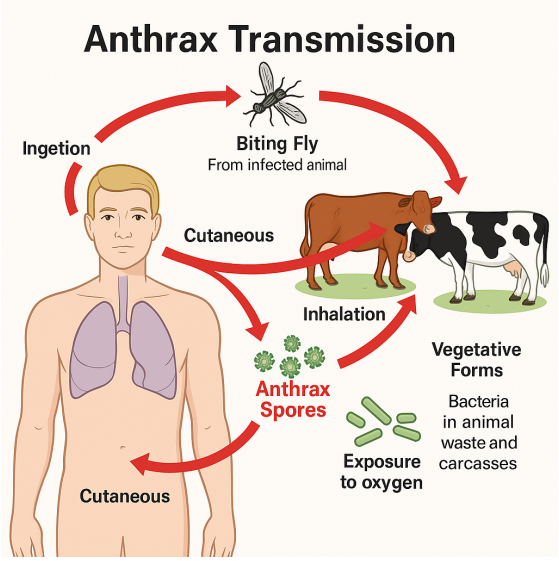

Figure 1: Modes of transmission of anthrax.

anism, providing deeper insights into the stability and progression of the disease. Also, Alfwzan et al. [2] introduced an unconventional computational methodology aimed at improving the accuracy of model predictions, evaluating potential control strategies, and identifying critical parameters that drive the dynamics of stochastic anthrax epidemics. Bylaiah et al. [3] utilized advanced machine learning techniques to create a predictive model for assessing anthrax risk, demonstrating how variations in environmental factors such as precipitation levels can influence disease outbreaks.

On the other hand, Helikumi, Lolika, and Mushayabasa [12] highlighted the significance of the basic reproduction number and its implications in simulating and understanding a wide range of infectious diseases, including anthrax. Mackey and Kribs [23] investigated the modeling of disease spread among zebra populations, providing valuable insights into the spatial and temporal patterns of anthrax transmission in wildlife. A proposition of a novel framework to evaluate the effectiveness of public health strategies for anthrax prevention, integrating decision-making processes related to health security have been proposed by Chen et al. [4]. Stella et al. [35] developed an SIR-based model to describe the transmission dynamics of anthrax within animal communities. Croicu [5] proposed the IACN model, which incorporated compartments representing infected animals, carcasses, and environmental reservoirs to better capture the ecological complexity of herbivore anthrax transmission. Osman, Makinde, and Theuri [28] provided an enhanced mathematical analysis of anthrax dynamics, offering qualitative insights and valuable implications for disease forecasting and control measures. Van den Driessche [37] emphasized

the importance of mathematical modeling as a critical tool for understanding the spread and control of infectious diseases, including anthrax.

Pantha, Day, and Lenhart [29] explored optimal control strategies within their mathematical framework, identifying approaches to effectively manage anthrax outbreaks through targeted interventions. Roy, van den Driessche, and Yakubu [32] developed a model to investigate how the growth and persistence of Bacillus anthracis spores in the environment affect fluctuations in susceptible animal populations. In addition, Kar and Batabyal [20] incorporated optimal control theory into their analysis of a nonlinear SIR epidemic model, emphasizing the role of vaccination as a key component in reducing the burden of the disease. Oh et al. [27] presented an analysis of a mathematical model specifically focused on gastrointestinal anthrax, shedding light on the transmission mechanisms and potential intervention strategies for this form of the disease. Finally, Karginov et al. [21] examined therapeutic approaches, modeling the combined effects of ciprofloxacin and antibody treatments in controlling bacterial growth and improving recovery outcomes.

Building on previous studies that develop models to analyze the transmission dynamics of anthrax, this work introduces a numerical approach that leverages the synergy between the Genocchi polynomials framework and the quasilinearization method (QLM). Earlier models in the literature have offered valuable insights into anthrax epidemiology using deterministic, stochastic, or optimal control frameworks. However, these models often rely on traditional numerical solvers and do not fully exploit advanced approximation techniques capable of handling nonlinearities with high accuracy and stability. Motivated by these gaps, our study presents a refined and computationally efficient framework that not only enhances the accuracy of solutions but also provides a robust foundation for sensitivity and control analysis of anthrax disease dynamics.

The main contributions and novelty of this work can be summarized as follows:

1. A complete analyze of an extended four-compartment anthrax transmission model, incorporating the interactions between susceptible, infected, recovered, and vaccinated animal populations, while capturing key biological processes such as disease-induced mortality, immunity waning, and demographic effects.

2. A hybrid Genocchi-quasilinearization method (Genocchi-QLM) is proposed, which is a numerical scheme that transforms the nonlinear system into a sequence of linear systems efficiently approximated by shifted Genocchi polynomials. To the best of our knowledge, this approach has not been previously applied to anthrax epidemiological models.

3. A rigorous convergence and error analysis is conducted, theoretically establishing the uniform convergence of the method and validating its accuracy through a residual error function technique.

4. We perform an extensive comparative validation to `ode45`, demonstrating the accuracy, efficiency, and stability of the Genocchi-QLM in capturing the dynamics of the model.

5. Real-world validation of the results confirms the ability of the method to provide highly accurate and reliable outcomes for the simulations.

6. Through comprehensive numerical experiments, we investigate the sensitivity of the system to key parameters, providing insights into the impact of vaccination strategies, recovery rates, and immunity waning on disease persistence and control.

The organization of this paper is as follows: In section 2, we present the mathematical model of anthrax disease in animals and define the underlying assumptions. Section 2 provides a review of Genocchi polynomials and then the shifted Genocchi polynomials with the error analysis. In addition to discussing the QLM for the anthrax model, section 4 presents the Genocchi collocation method, which is based on the quasilinearization approach with residual error. Numerical simulation results are presented in section 5, emphasizing the impact of significant parameters on disease control and transmission. At last, a conclusion to the paper is presented in section 6.

2 Model formulation

In this section, we need to construct a nonlinear mathematical model of the anthrax disease model in animals. To formulate the proposed model, let us subdivide the total number of population $N(t)$ at time t into four mutually exclusive classes such as: $S(t)$, which represents the number of susceptible animals that are at risk of contracting anthrax, while $I(t)$ denotes the infected animals exhibiting clinical symptoms of the disease. The $R(t)$ compartment accounts for recovered animals that have survived infection and acquired temporary or partial immunity. The final compartment, $V(t)$, represents the vaccinated animal population, which has gained immunity through preventive vaccination programs. Thus, the final model can be considered as follows [33, 9]:

$$\begin{aligned}
\frac{dS(t)}{dt} &= \eta - \alpha I(t)S(t) - (\beta+\gamma)S(t) + \varepsilon V(t) + \theta R(t),\\
\frac{dI(t)}{dt} &= \alpha I(t)S(t) - (\beta+\mu+\lambda)I(t),\\
\frac{dR(t)}{dt} &= \lambda I(t) - (\beta+\theta)R(t),\\
\frac{dV(t)}{dt} &= \gamma S(t) - (\beta+\varepsilon)V(t),
\end{aligned} \tag{1}$$

with the initial conditions

$$S(0) = S_0, \quad I(0) = I_0, \quad R(0) = R_0, \quad V(0) = V_0. \tag{2}$$

The description of the parameters of the model is given in Table 1, while Figure 2 represents the flowchart diagram of the anthrax disease model. In the next section, we will provide the fundamentals of the Genocchi polynomials.

Table 1: Declaration of parameters for the anthrax disease model.

Parameters	**Description**
η	Rate of recruitment
α	Rate of contact
β	Rate of natural death
γ	Rate of vaccination
θ	The waning rate of recovery
ε	The waning immunity rate of vaccinated animals
μ	Rate of induced-disease death
λ	The recovery rate of animals

3 Fundamentals of Genocchi polynomials

In this section, we first demonstrate the overview of Genocchi polynomials with significant properties on the interval $[0, 1]$. Then, we shift the interval to general form $[0, b]$ to get the modified Genocchi polynomials and present the error analysis.

3.1 Fundamental features of Genocchi polynomials

The Genocchi polynomials and the Genocchi numbers can be defined by the generating functions as follows [15, 8]:

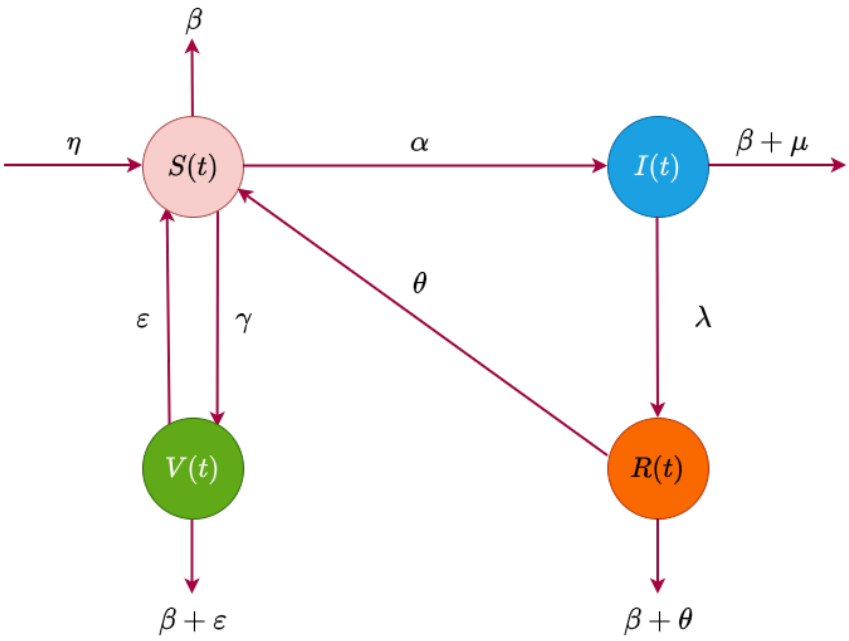

Figure 2: The flowchart for the anthrax disease model.

$$\frac{2xe^{x\tau}}{e^x+1}=\sum_{q=0}^{\infty}G_q(\tau)\frac{x^q}{q!},\quad (|x|<\pi), \tag{3}$$

$$\frac{2x}{e^x+1}=\sum_{q=0}^{\infty}G_q\frac{x^q}{q!},\quad (|x|<\pi). \tag{4}$$

Definition 1. The Genocchi polynomials $G_q(\tau)$ of degree q on the interval $[0,1]$ are defined as follows:

$$G_q(\tau)=\sum_{k=0}^{q}\binom{q}{k}G_k\,\tau^{q-k}, \tag{5}$$

where G_k represents the Genocchi numbers, which are connected with Bernoulli numbers in the following way:

$$G_q=2(1-2^q)B_q,\quad q>1. \tag{6}$$

The following equations are some of the many interesting characteristics of the Genocchi polynomials:

$$\frac{d}{d\tau}G_q(\tau)=q\,G_{q-1}(\tau),\quad q\geq 1, \tag{7}$$

$$G_q(\tau+1)+G_q(\tau)=2\,q\,\tau^{q-1},\quad q\geq 1, \tag{8}$$

$$G_q(1)+G_q(0)=0,\quad q>1. \tag{9}$$

Let us represent the $(Q+1)$ vector of Genocchi polynomials by

$$\boldsymbol{G}_Q(\tau)=\left[G_1(\tau)\;G_2(\tau)\;\ldots\;G_{Q+1}(\tau)\right]. \tag{10}$$

We can deduce from this representation the following lemma.

Lemma 1. The mathematical matrix representation for $\boldsymbol{G}_Q(\tau)$ satisfies

$$\boldsymbol{G}_Q(\tau)=\boldsymbol{\Delta}_Q(\tau)\boldsymbol{M}, \tag{11}$$

where

$$\boldsymbol{\Delta}_Q(\tau)=\left[1\;\tau\;\tau^2\;\ldots\;\tau^Q\right],$$

and

$$\boldsymbol{M}=\begin{bmatrix} \binom{1}{1}G_1 & \binom{2}{2}G_2 & \binom{3}{3}G_3 & \ldots & \binom{Q}{Q}G_Q & \binom{Q+1}{Q+1}G_{Q+1}\\ 0 & \binom{2}{1}G_1 & \binom{3}{2}G_2 & \ldots & \binom{Q}{Q-1}G_{Q-1} & \binom{Q+1}{Q}G_Q\\ 0 & 0 & \binom{3}{1}G_1 & \ldots & \binom{Q}{Q-2}G_{Q-2} & \binom{Q+1}{Q-1}G_{Q-1}\\ \vdots & \vdots & \vdots & \ddots & \vdots & \vdots\\ 0 & 0 & 0 & \ldots & \binom{Q}{1}G_1 & \binom{Q+1}{2}G_2\\ 0 & 0 & 0 & \ldots & \ldots & \binom{Q+1}{1}G_1 \end{bmatrix}_{(Q+1)\times(Q+1)}. \tag{12}$$

3.2 Modified Genocchi polynomials on the interval $[0, b]$

The approximate solution of function for interval $[0,1]$ in terms of Genocchi polynomials is expressed as

$$\Psi_Q(\tau)=\sum_{k=1}^{Q+1}\varphi_k G_k(\tau),\qquad \tau\in[0,1]. \tag{13}$$

To obtain the shifted version of Genocchi polynomials, we replace τ by t/b in the matrix $\boldsymbol{G}_Q(\tau)$.

Definition 2. The shifted Genocchi polynomials on $[0,b]$ is defined via relation

$$\boldsymbol{G}_Q(t)=\boldsymbol{\Delta}_Q(t)\boldsymbol{M},\qquad t\in[0,b], \tag{14}$$

where

$$\boldsymbol{\Delta}_Q(t) = \left[1 \; t/b \; (t/b)^2 \; \ldots \; (t/b)^Q\right], \tag{15}$$

so the approximate solution of the function on the interval $[0, b]$ is given by

$$\Psi_Q(t) = \sum_{k=1}^{Q+1} \varphi_k G_k(t), \qquad t \in [0, b]. \tag{16}$$

3.3 Error analysis on the interval $[0, b]$

In this section, we expand the error analysis of the Genocchi polynomials approximation from the unit interval $[0, 1]$ to a broad finite interval $[0, b]$, where $b > 0$. Assume first that the approximated function $g(t)$ is an arbitrary element of $H = L^2[0, b]$ and

$$\Pi = span\{G_1(t), G_2(t), \ldots, G_{Q+1}(t)\} \subset H,$$

where $\{G_k(t)\}_{k=1}^{Q+1}$ denotes the shifted Genocchi polynomials on $[0, b]$. We can state that $g(t)$ has a unique best approximation $g^*(t)$ in the space Π such that for all $\Psi(t) \in \Pi$,

$$\|g(t) - g^*(t)\|_2 \leq \|g(t) - \Psi(t)\|_2 . \tag{17}$$

Since $g^*(t) \in \Pi$, there exists a unique set of coefficients $\{\varphi_k\}_{k=1}^{Q+1}$ such that

$$g(t) \cong g^*(t) = \sum_{k=1}^{Q+1} \varphi_k G_k(t) = \boldsymbol{G}(t)\boldsymbol{\Phi},$$

where $\boldsymbol{\Phi} = \left[\varphi_1 \; \varphi_2 \; \ldots \; \varphi_{Q+1}\right]^T$, $\boldsymbol{G}(t) = \left[G_1(t) \; G_2(t) \; \ldots \; G_{Q+1}(t)\right]$. The following lemma is required in order to determine the values of the coefficients.

Lemma 2. Assume that $g \in C^Q[0, b]$ can be approximated by the Genocchi series $\sum_{k=1}^{Q+1} \varphi_k G_k(t)$. Then the unknown coefficients $\{\varphi_k\}_{k=1}^{Q+1}$ satisfy

$$\varphi_k = \frac{1}{2(k!)} \left(g^{(k-1)}(0) + g^{(k-1)}(b)\right).$$

Proof. The result follows from the properties of Genocchi polynomials in (8) and (9) for the interval $[0, b]$. Please refer to [14] for proof. □

Lemma 3. Suppose that $g(t) \in C^{(k+1)}[0,b]$ with $k \leq Q$ and that $\Pi = \text{span}\{G_1(t), G_2(t), \ldots, G_{Q+1}(t)\}$. If $\boldsymbol{G}(t)\boldsymbol{\Phi}$ is the best approximation of $g(t)$ from Π in the L^2-norm, then

$$\|\xi_{Q+1}(g)\| \leq \frac{b^{\frac{2k+3}{2}}\,\Theta}{(k+1)!\,\sqrt{2k+3}},$$

where

$$\xi_{Q+1}(g) = g(t) - \boldsymbol{G}(t)\boldsymbol{\Phi}, \quad \Theta = \max_{t\in[0,b]} |g^{(k+1)}(t)|.$$

Proof. In order to observe this, we set

$$\Psi_1(t) = g(0) + tg'(0) + \frac{t^2}{2!}g''(0) + \cdots + \frac{t^k}{k!}g^{(k)}(0).$$

It is evident from Taylor's expansion that

$$|g(t) - \Psi_1(t)| \leq \left|g^{(k+1)}(\xi_t)\right| \frac{(t)^{k+1}}{(k+1)!},$$

where $\xi_t \in [0,b]$. Since $\boldsymbol{G}(t)\boldsymbol{\Phi}$ is the best approximation of $g(t)$ out of Π and $\Psi_1(t) \in \Pi$, then from (17), we have

$$\begin{aligned}
\|g(t) - \boldsymbol{G}(t)\boldsymbol{\Phi}\|_{L_2}^2 \leq \|g(t) - \Psi_1(t)\|_{L_2}^2 &= \int_0^b |g(t) - \Psi_1(t)|^2 dt \\
&\leq \int_0^b |g^{(k+1)}(\xi_t)|^2 \left(\frac{t^{k+1}}{(k+1)!}\right)^2 dt \\
&\leq \frac{b^{2k+3}\,\Theta^2}{((k+1)!)^2\,(2k+3)}.
\end{aligned}$$

When we take square roots of both sides, we get

$$\|g(t) - \boldsymbol{G}(t)\boldsymbol{\Phi}\| \leq \frac{b^{\frac{2k+3}{2}}\,\Theta}{(k+1)!\,\sqrt{2k+3}};$$

this complete the proof. □

4 Quasilinearization technique

In this section, we will cover the main concept and steps of the recommended QLM. The goal of the QLM is to convert the original nonlinear model (1) into a set of linear equations. The Genocchi collocation method will next be applied to the linearized models that have been produced.

Here, we briefly outline the basic concepts that allow the QLM to solve our model problems; refer to [18, 16, 38, 1, 17] for more in-depth discussions and applications. Let us examine the nonlinear form (1), which represents the standard formulation of our model. To solve the system of equations (1), we need to first restate the anthrax disease model as

$$\dot{\boldsymbol{\Upsilon}}(t) = \boldsymbol{H}(t, \boldsymbol{\Upsilon}(t)), \tag{18}$$

where

$$\dot{\boldsymbol{\Upsilon}}(t) = \begin{bmatrix} \dot{S}(t) \\ \dot{I}(t) \\ \dot{R}(t) \\ \dot{V}(t) \end{bmatrix}, \quad \boldsymbol{\Upsilon}(t) = \begin{bmatrix} S(t) \\ I(t) \\ R(t) \\ V(t) \end{bmatrix},$$

$$\boldsymbol{H}(t, \boldsymbol{\Upsilon}(t)) = \begin{bmatrix} \eta - \alpha I(t)S(t) - (\beta + \gamma)S(t) + \theta R(t) + \varepsilon V(t) \\ \alpha I(t)S(t) - (\beta + \mu + \lambda)I(t) \\ \lambda I(t) - (\beta + \varepsilon)R(t) \\ \gamma S(t) - (\beta + \theta)V(t) \end{bmatrix}.$$

Next, select an initial approximation $\boldsymbol{\Upsilon}_0(t)$ for $\boldsymbol{\Upsilon}(t)$. Then, the QLM iteration for (18) is defined as follows:

$$\dot{\boldsymbol{\Upsilon}}_{\psi+1}(t) = \boldsymbol{H}(t, \boldsymbol{\Upsilon}_\psi(t)) + (\boldsymbol{\Upsilon}_{\psi+1}(t) - \boldsymbol{\Upsilon}_\psi(t))\boldsymbol{H}_{\boldsymbol{\Upsilon}}(t, \boldsymbol{\Upsilon}_\psi(t)), \quad \psi = 0, 1, \ldots, \tag{19}$$

with the initial conditions as mentioned in (2). The functional derivatives of $\boldsymbol{H}(t, \boldsymbol{\Upsilon}(t))$ are demonstrated by the (4×4) Jacobian matrix of anthrax system (18). The following linearized model form is produced after the QLM approach is applied to the nonlinear model (18) as follows:

$$\dot{\boldsymbol{\Upsilon}}_{\psi+1}(t) + \boldsymbol{E}_\psi(t)\, \boldsymbol{\Upsilon}_{\psi+1}(t) = \boldsymbol{\Sigma}_\psi(t), \qquad \psi = 0, 1, \ldots, \tag{20}$$

where

$$\boldsymbol{E}_\psi(t) = \begin{bmatrix} \alpha I_\psi(t) + \beta + \gamma & \alpha S_\psi(t) & -\theta & -\varepsilon \\ -\alpha I_\psi(t) & -\alpha S_\psi(t) + \beta + \mu + \lambda & 0 & 0 \\ 0 & -\lambda & \beta + \theta & 0 \\ -\gamma & 0 & 0 & \beta + \varepsilon \end{bmatrix},$$

$$\boldsymbol{\Sigma}_\psi(t) = \begin{bmatrix} \eta + \alpha S_\psi(t) I_\psi(t) \\ -\alpha S_\psi(t) I_\psi(t) \\ 0 \\ 0 \end{bmatrix},$$

with the initial conditions given by

$$\boldsymbol{\Upsilon}_{\psi+1}(0) = \begin{bmatrix} S_{\psi+1}(0) \\ I_{\psi+1}(0) \\ R_{\psi+1}(0) \\ V_{\psi+1}(0) \end{bmatrix} = \begin{bmatrix} S_0 \\ I_0 \\ R_0 \\ V_0 \end{bmatrix}. \tag{21}$$

Therefore, we solve the quasilinear model (20) using the Genocchi collocation method instead of solving the original model (1). The last method is called Genocchi-QLM.

4.1 Genocchi-QLM

Here, we aim to solve the system of linearized initial-value problems in (20) and (21) on the interval $[0, b]$ using Genocchi-QLM. To continue, we suppose that the truncated Genocchi polynomials series form (16) can be used to express the solutions of model (20). At iteration $\psi \geq 0$, these approximations can be written as follows:

$$\begin{aligned} S_Q^{\psi+1}(t) &= \sum_{k=1}^{Q+1} \varphi_{k,1}^{\psi} G_k(t) = \boldsymbol{G}_Q(t)\boldsymbol{\Phi}_{Q,1}^{\psi}, \\ I_Q^{\psi+1}(t) &= \sum_{k=1}^{Q+1} \varphi_{k,2}^{\psi} G_k(t) = \boldsymbol{G}_Q(t)\boldsymbol{\Phi}_{Q,2}^{\psi}, \\ R_Q^{\psi+1}(t) &= \sum_{k=1}^{Q+1} \varphi_{k,3}^{\psi} G_k(t) = \boldsymbol{G}_Q(t)\boldsymbol{\Phi}_{Q,3}^{\psi}, \\ V_Q^{\psi+1}(t) &= \sum_{k=1}^{Q+1} \varphi_{k,4}^{\psi} G_k(t) = \boldsymbol{G}_Q(t)\boldsymbol{\Phi}_{Q,4}^{\psi}, \end{aligned} \tag{22}$$

where $\boldsymbol{\Phi}_{Q,\upsilon}^{\psi}$ represents the vectors of unknown coefficients associated with each approximate solution and is given by

$$\boldsymbol{\Phi}_{Q,\upsilon}^{\psi} = \left[\varphi_{1,\upsilon}^{\psi}\ \varphi_{2,\upsilon}^{\psi}\ \ldots\ \varphi_{Q+1,\upsilon}^{\psi}\right]^T, \quad \upsilon = 1, 2, 3, 4.$$

The representation of $\boldsymbol{G}_Q(t)$ in (14) enables us to reconstruct the relations in (22) as follows:

$$\begin{aligned} S_Q^{\psi+1}(t) &= \boldsymbol{\Delta}_Q(t)\, \boldsymbol{M}\, \boldsymbol{\Phi}_{Q,1}^{\psi}, \qquad I_Q^{\psi+1}(t) = \boldsymbol{\Delta}_Q(t)\, \boldsymbol{M}\, \boldsymbol{\Phi}_{Q,2}^{\psi}, \\ R_Q^{\psi+1}(t) &= \boldsymbol{\Delta}_Q(t)\, \boldsymbol{M}\, \boldsymbol{\Phi}_{Q,3}^{\psi}, \qquad V_Q^{\psi+1}(t) = \boldsymbol{\Delta}_Q(t)\, \boldsymbol{M}\, \boldsymbol{\Phi}_{Q,4}^{\psi}. \end{aligned} \tag{23}$$

Next, we deduce the first derivative of approximate solutions in (23) by the following relations:

$$\begin{aligned} \dot{S}_Q^{\psi+1}(t) &= \boldsymbol{\Delta}_Q(t)\, \boldsymbol{D}\, \boldsymbol{M}\, \boldsymbol{\Phi}_{Q,1}^{\psi}, \qquad \dot{I}_Q^{\psi+1}(t) = \boldsymbol{\Delta}_Q(t)\, \boldsymbol{D}\, \boldsymbol{M}\, \boldsymbol{\Phi}_{Q,2}^{\psi}, \\ \dot{R}_Q^{\psi+1}(t) &= \boldsymbol{\Delta}_Q(t)\, \boldsymbol{D}\, \boldsymbol{M}\, \boldsymbol{\Phi}_{Q,3}^{\psi}, \qquad \dot{V}_Q^{\psi+1}(t) = \boldsymbol{\Delta}_Q(t)\, \boldsymbol{D}\, \boldsymbol{M}\, \boldsymbol{\Phi}_{Q,4}^{\psi}, \end{aligned} \tag{24}$$

where $\boldsymbol{D}$ is the differentiation matrix of Genocchi polynomials and is defined as follows:

$$\boldsymbol{D} = \frac{1}{b} \begin{bmatrix} 0 & 2 & 0 & \cdots & 0 \\ 0 & 0 & 3 & \cdots & 0 \\ \vdots & \vdots & \vdots & \ddots & \vdots \\ 0 & 0 & 0 & \cdots & Q+1 \\ 0 & 0 & 0 & \cdots & 0 \end{bmatrix}_{(Q+1)\times(Q+1)}. \tag{25}$$

Now, we are interested in the matrix representations of $\boldsymbol{\Upsilon}_{\psi+1}(t)$ and $\dot{\boldsymbol{\Upsilon}}_{\psi+1}(t)$ in (20). So we have the following matrix representations:

$$\begin{aligned} \bar{\boldsymbol{\Delta}}_Q(t) &= \begin{bmatrix} \boldsymbol{\Delta}_Q(t) & \mathbf{0} & \mathbf{0} & \mathbf{0} \\ \mathbf{0} & \boldsymbol{\Delta}_Q(t) & \mathbf{0} & \mathbf{0} \\ \mathbf{0} & \mathbf{0} & \boldsymbol{\Delta}_Q(t) & \mathbf{0} \\ \mathbf{0} & \mathbf{0} & \mathbf{0} & \boldsymbol{\Delta}_Q(t) \end{bmatrix}, \quad \bar{\boldsymbol{\Phi}}_Q^{\psi} = \begin{bmatrix} \boldsymbol{\Phi}_{Q,1}^{\psi} \\ \boldsymbol{\Phi}_{Q,2}^{\psi} \\ \boldsymbol{\Phi}_{Q,3}^{\psi} \\ \boldsymbol{\Phi}_{Q,4}^{\psi} \end{bmatrix}, \\ \bar{\boldsymbol{M}} &= \begin{bmatrix} \boldsymbol{M} & \mathbf{0} & \mathbf{0} & \mathbf{0} \\ \mathbf{0} & \boldsymbol{M} & \mathbf{0} & \mathbf{0} \\ \mathbf{0} & \mathbf{0} & \boldsymbol{M} & \mathbf{0} \\ \mathbf{0} & \mathbf{0} & \mathbf{0} & \boldsymbol{M} \end{bmatrix}, \quad \bar{\boldsymbol{D}} = \begin{bmatrix} \boldsymbol{D} & \mathbf{0} & \mathbf{0} & \mathbf{0} \\ \mathbf{0} & \boldsymbol{D} & \mathbf{0} & \mathbf{0} \\ \mathbf{0} & \mathbf{0} & \boldsymbol{D} & \mathbf{0} \\ \mathbf{0} & \mathbf{0} & \mathbf{0} & \boldsymbol{D} \end{bmatrix}. \end{aligned} \tag{26}$$

Then, the approximate solutions $\boldsymbol{\Upsilon}_{\psi+1}(t)$ and $\dot{\boldsymbol{\Upsilon}}_{\psi+1}(t)$ can be expressed in matrix forms as follows:

$$\boldsymbol{\Upsilon}_{\psi+1}(t) = \bar{\boldsymbol{\Delta}}_Q(t)\, \bar{\boldsymbol{M}}\, \bar{\boldsymbol{\Phi}}_Q^{\psi}, \qquad \dot{\boldsymbol{\Upsilon}}_{\psi+1}(t) = \bar{\boldsymbol{\Delta}}_Q(t)\, \bar{\boldsymbol{D}}\, \bar{\boldsymbol{M}}\, \bar{\boldsymbol{\Phi}}_Q^{\psi}. \tag{27}$$

By using the collocation points defined as

$$t_i = \frac{i\, b}{Q}, \qquad i = 0, 1, \ldots, Q, \tag{28}$$

in linear model (20), we obtain

$$\dot{\boldsymbol{\Upsilon}}_{\psi+1}(t_i) + \boldsymbol{E}_{\psi}(t_i)\, \boldsymbol{\Upsilon}_{\psi+1}(t_i) = \boldsymbol{\Sigma}_{\psi}(t_i), \qquad i = 0, 1, \ldots, Q, \tag{29}$$

which can be simplified as follows:

$$\breve{\dot{\boldsymbol{\Upsilon}}}_{\psi+1} + \breve{\boldsymbol{E}}_{\psi}\, \breve{\boldsymbol{\Upsilon}}_{\psi+1} = \breve{\boldsymbol{\Sigma}}_{\psi}, \tag{30}$$

where

$$\breve{\dot{\boldsymbol{\Upsilon}}}_{\psi+1} = \begin{bmatrix} \dot{\boldsymbol{\Upsilon}}_{\psi+1}(t_0) \\ \dot{\boldsymbol{\Upsilon}}_{\psi+1}(t_1) \\ \vdots \\ \dot{\boldsymbol{\Upsilon}}_{\psi+1}(t_Q) \end{bmatrix}, \quad \breve{\boldsymbol{E}}_{\psi} = \begin{bmatrix} \boldsymbol{E}_{\psi}(t_0) & \mathbf{0} & \cdots & \mathbf{0} \\ \mathbf{0} & \boldsymbol{E}_{\psi}(t_1) & \cdots & \mathbf{0} \\ \vdots & \vdots & \ddots & \vdots \\ \mathbf{0} & \mathbf{0} & \cdots & \boldsymbol{E}_{\psi}(t_Q) \end{bmatrix},$$

$$\breve{\boldsymbol{\Upsilon}}_{\psi+1} = \begin{bmatrix} \boldsymbol{\Upsilon}_{\psi+1}(t_0) \\ \boldsymbol{\Upsilon}_{\psi+1}(t_1) \\ \vdots \\ \boldsymbol{\Upsilon}_{\psi+1}(t_Q) \end{bmatrix}, \quad \breve{\boldsymbol{\Sigma}}_{\psi} = \begin{bmatrix} \boldsymbol{\Sigma}_{\psi}(t_0) \\ \boldsymbol{\Sigma}_{\psi}(t_1) \\ \vdots \\ \boldsymbol{\Sigma}_{\psi}(t_Q) \end{bmatrix}.$$

For the matrix representation of $\breve{\dot{\boldsymbol{\Upsilon}}}_{\psi+1}$ and $\breve{\boldsymbol{\Upsilon}}_{\psi+1}$, we need the following lemma.

Lemma 4. The matrices $\breve{\boldsymbol{\Upsilon}}_{\psi+1}$ and $\breve{\dot{\boldsymbol{\Upsilon}}}_{\psi+1}$, produced from using collocation points (28) in $\boldsymbol{\Upsilon}_{\psi+1}(t_i)$ and $\dot{\boldsymbol{\Upsilon}}_{\psi+1}(t_i)$, can be constructed as follows:

$$\breve{\boldsymbol{\Upsilon}}_{\psi+1} = \breve{\boldsymbol{\Delta}}_{Q}\, \bar{\boldsymbol{M}}\, \bar{\boldsymbol{\Phi}}_{Q}^{\psi}, \qquad \breve{\dot{\boldsymbol{\Upsilon}}}_{\psi+1} = \breve{\boldsymbol{\Delta}}_{Q}\, \bar{\boldsymbol{D}}\, \bar{\boldsymbol{M}}\, \bar{\boldsymbol{\Phi}}_{Q}^{\psi}, \tag{31}$$

where

$$\breve{\boldsymbol{\Delta}}_{Q} = \begin{bmatrix} \bar{\boldsymbol{\Delta}}_{Q}(t_0) & \mathbf{0} & \cdots & \mathbf{0} \\ \mathbf{0} & \bar{\boldsymbol{\Delta}}_{Q}(t_1) & \cdots & \mathbf{0} \\ \vdots & \vdots & \ddots & \vdots \\ \mathbf{0} & \mathbf{0} & \cdots & \bar{\boldsymbol{\Delta}}_{Q}(t_Q) \end{bmatrix}. \tag{32}$$

By using (31) into (29), we obtain the matrix form of the linear model as follows:

$$\breve{\boldsymbol{\Delta}}_{Q}\, \bar{\boldsymbol{D}}\, \bar{\boldsymbol{M}}\, \bar{\boldsymbol{\Phi}}_{Q}^{\psi} + \breve{\boldsymbol{E}}_{\psi}\, \breve{\boldsymbol{\Delta}}_{Q}\, \bar{\boldsymbol{M}}\, \bar{\boldsymbol{\Phi}}_{Q}^{\psi} = \breve{\boldsymbol{\Sigma}}_{\psi}, \tag{33}$$

which can be rewritten in the form:

$$\boldsymbol{\Xi}_{\psi+1}\, \bar{\boldsymbol{\Phi}}_{Q}^{\psi} = \breve{\boldsymbol{\Sigma}}_{\psi}, \qquad or \qquad [\boldsymbol{\Xi}_{\psi+1}; \breve{\boldsymbol{\Sigma}}_{\psi}], \tag{34}$$

where

$$\boldsymbol{\Xi}_{\psi+1} = \breve{\boldsymbol{\Delta}}_{Q}\, \bar{\boldsymbol{D}}\, \bar{\boldsymbol{M}} + \breve{\boldsymbol{E}}_{\psi}\, \breve{\boldsymbol{\Delta}}_{Q}\, \bar{\boldsymbol{M}}.$$

At last, the matrix representation of the initial conditions, given in (2), is produced when tending $t \to 0$ in (27) as follows:

$$\bar{\boldsymbol{\Delta}}_Q(0)\,\bar{\boldsymbol{M}}\,\bar{\boldsymbol{\Phi}}_Q^{\psi} = \boldsymbol{B}_0^{\psi+1}, \tag{35}$$

where $\boldsymbol{B}_0^{\psi+1}$ is given in (21). After approximate the initial solution of model $\boldsymbol{\Upsilon}_0(t)$, we replace the first four rows of (34) with (35) to obtain the new augmented matrix

$$[\mathring{\bar{\boldsymbol{\Xi}}}_{\psi+1}; \mathring{\bar{\boldsymbol{\Sigma}}}_{\psi}]. \tag{36}$$

By solving this system of linear equations, we obtain the unknown coefficients $\boldsymbol{\Phi}_Q^{\psi}$, which are used to gain the four approximations of the anthrax disease model in (1).

4.2 Residual error functions

In this subsection, we further validate the results by calculating the residual error for the model (1). Validating the accuracy of the provided collocation technique is essential in this case. Let $Res_Q^{\psi+1}(t)$ represent the residual error function. As a result, we obtain

$$\begin{aligned}
Res_{S,Q}^{\psi+1}(t) &= |\dot{S}_Q^{\psi+1}(t) - \eta + \alpha I_Q^{\psi+1}(t) S_Q^{\psi+1}(t) + (\beta+\gamma) S_Q^{\psi+1}(t) - \theta R_Q^{\psi+1}(t) \\
&\quad - \varepsilon V_Q^{\psi+1}(t)| \cong 0, \\
Res_{I,Q}^{\psi+1}(t) &= |\dot{I}_Q^{\psi+1}(t) - \alpha I_Q^{\psi+1}(t) S_Q^{\psi+1}(t) + (\beta+\mu+\lambda) I_Q^{\psi+1}(t)| \cong 0, \\
Res_{R,Q}^{\psi+1}(t) &= |\dot{R}_Q^{\psi+1}(t) - \lambda I_Q^{\psi+1}(t) + (\beta+\theta) R_Q^{\psi+1}(t)| \cong 0, \\
Res_{V,Q}^{\psi+1}(t) &= |\dot{V}_Q^{\psi+1}(t) - \gamma S_Q^{\psi+1}(t) + (\beta+\varepsilon) V_Q^{\psi+1}(t)| \cong 0,
\end{aligned} \tag{37}$$

where $\psi = 0, 1, \ldots, 5$. Indeed, at the collocation points specified in (28), the residual error function $Res_Q^{\psi+1}(t)$ becomes zero. As a result, we anticipate that as Q increases, the residual error $Res_Q^{\psi+1}(t)$ converges to zero, ensuring that the approximate solution becomes increasingly accurate.

5 Numerical simulations and validation

5.1 Numerical results

In this subsection, we present the numerical results for the nonlinear anthrax disease model in animals, considering two cases. The suggested Genocchi-QLM is used to run the simulations, proving the method's effectiveness and dependability. To ensure the accuracy and consistency of the results, MATLAB 2023 is used for all calculations and simulations.

Example 1. Consider the following values of parameters in the first case of the anthrax disease model [33]:

$$\eta = 200, \quad \alpha = 0.0001, \quad \gamma = 0.1, \quad \beta = 0.001,$$
$$\theta = 0.02, \quad \varepsilon = 0.02, \quad \mu = 0.1, \quad \lambda = 0.01,$$

where the initial conditions are

$$S(0) = 0.2, \quad I(0) = 0.3, \quad R(0) = 0.4, \quad V(0) = 0.5.$$

In the iterated Genocchi-QLM procedure, by setting $\psi = 5$ and using $\boldsymbol{\Upsilon}_0(t) = 0$ as the initial approximation for the linearized system (20) with $Q = 20$ and a simulation time of $b = 50$, the dynamics of the approximate solutions for the susceptible, infected, recovered, and vaccinated populations are illustrated in Figures 3a, 4a, 5a, and 6a, respectively, with CPU time 20.648 sec. For validation purposes, the results obtained from the classical `ode45` solver in MATLAB are also presented for comparison. As observed, the numerical solutions generated by the Genocchi-QLM method exhibit an excellent agreement with those produced by `ode45`, confirming the reliability and accuracy of the proposed approach. Furthermore, the corresponding residual errors for each population class —susceptible, infected, recovered, and vaccinated— are depicted in Figures 3b, 4b, 5b, and 6b, respectively, demonstrating the high accuracy and convergence of the Genocchi-QLM technique across all compartments.

From a physical perspective, the results reflect the expected epidemiological behavior of anthrax transmission. The susceptible population $S(t)$ initially rises due to constant recruitment ($\eta = 200$) before stabilizing as infection, recovery, and vaccination interact to balance the dynamics. The infected population $I(t)$ steadily declines over time, driven by recovery ($\lambda = 0.01$) and disease-induced mortality ($\mu = 0.1$), highlighting the importance of control interventions to reduce infection levels. The recovered population $R(t)$ grows moderately, reflecting successful recoveries, while waning immunity ($\theta = 0.02$) allows some individuals to transition back into the susceptible pool, sustaining a low-level risk of reinfection. Similarly, the vaccinated population

$V(t)$ increases rapidly in the early phase due to a relatively high vaccination rate ($\gamma = 0.1$) before stabilizing, with waning immunity ($\varepsilon = 0.02$) gradually reintroducing a portion of vaccinated individuals into susceptibility. These trends collectively underscore the role of effective vaccination strategies and the need for continuous monitoring to manage disease persistence in animal populations.

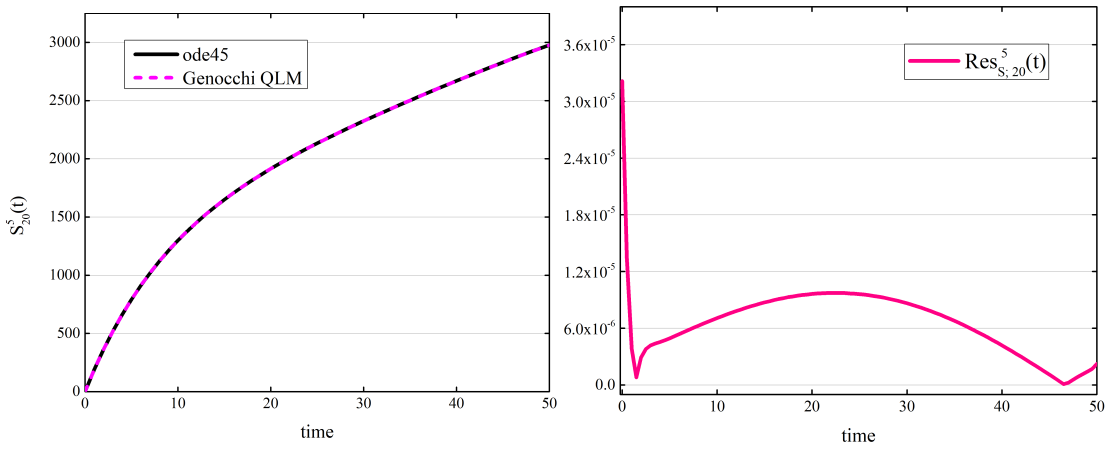

(a) $S^5_{20}(t)$ and `ode45` (b) $Res^5_{S,20}(t)$

Figure 3: The approximate and `ode45` solutions of $S(t)$ for $Q = 20$ (3a) and the residual error (3b) for $\psi = 5$ in Example 1.

Example 2. In the next case of the anthrax disease model, consider the following values of parameters [9]:

$$\eta = 200, \quad \alpha = 0.0001, \quad \gamma = 0.1, \quad \beta = 0.001,$$
$$\theta = 0.02, \quad \varepsilon = 0.003, \quad \mu = 0.1, \quad \lambda = 0.01,$$

where the initial conditions are

$$S(0) = 2000, \quad I(0) = 100, \quad R(0) = 300, \quad V(0) = 500.$$

Figures 7a, 8a, 9a, and 10a, respectively, show the results of approximate solutions for $S(t)$, $I(t)$, $R(t)$, and $V(t)$ obtained via the Genocchi-QLM method for $Q = 20$, simulation time $b = 50$, and iterated QLM with $\psi = 5$. Additionally, the results obtained from the classical `ode45` solver are presented for validation. As observed, the approximate solutions generated by the Genocchi-QLM approach show excellent agreement with those of `ode45`, confirming the accuracy and

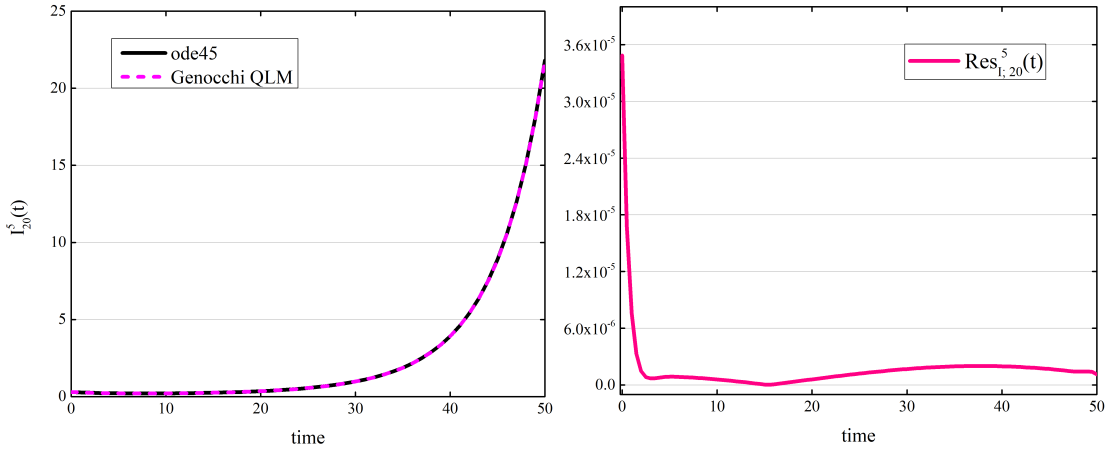

(a) $I^5_{20}(t)$ and `ode45` (b) $Res^5_{I,20}(t)$

Figure 4: The approximate and `ode45` solutions of $I(t)$ for $Q = 20$ (4a) and the residual error (4b) for $\psi = 5$ in Example 1.

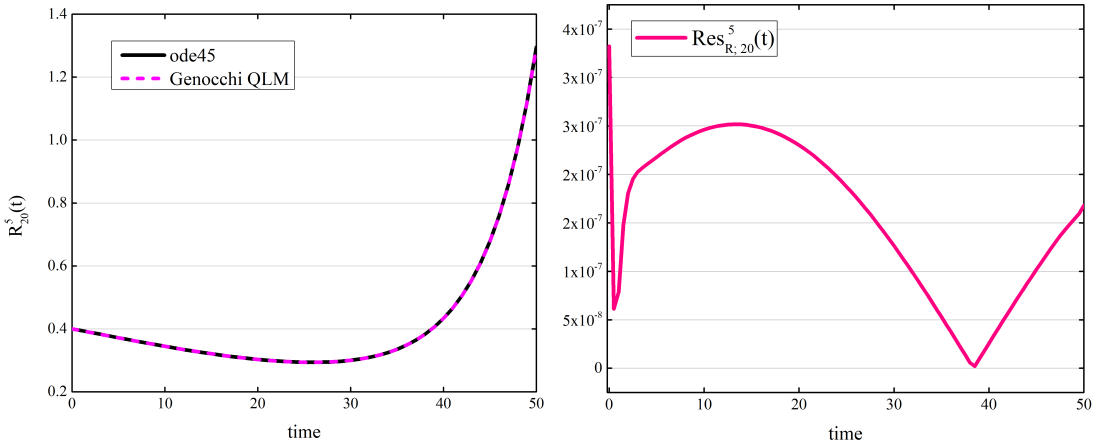

(a) $R^5_{20}(t)$ and `ode45` (b) $Res^5_{R,20}(t)$

Figure 5: The approximate and `ode45` solutions of $R(t)$ for $Q = 20$ (5a) and the residual error (5b) for $\psi = 5$ in Example 1.

stability of the proposed numerical technique. The residual errors for susceptible, infected, recovered, and vaccinated populations are shown in Figures 7b, 8b, 9b, and 10b with CPU time 20.113 sec, demonstrating the high precision and convergence behavior of the Genocchi-QLM method.

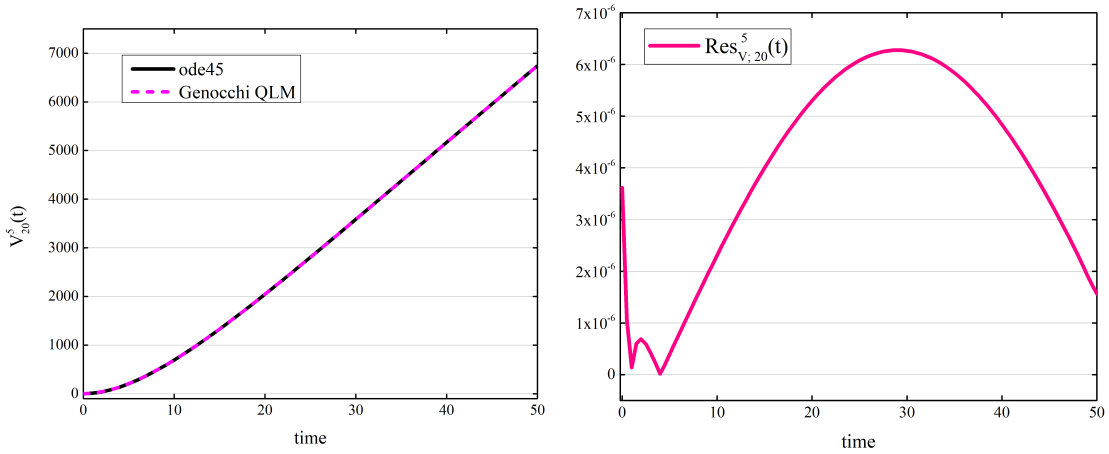

(a) $V_{20}^5(t)$ and `ode45` (b) $Res_{V,20}^5(t)$

Figure 6: The approximate and `ode45` solutions of $V(t)$ for $Q = 20$ (6a) and the residual error (6b) for $\psi = 5$ in Example 1.

From a physical perspective, the second example highlights more pronounced dynamic changes compared to the first case, reflecting the impact of parameter adjustments on disease transmission. The susceptible population $S(t)$ initially increases but stabilizes at a lower level, indicating stronger transmission or reduced vaccination coverage in this scenario. The infected population $I(t)$ displays a slower decline, suggesting either a reduced recovery rate or higher persistence of infection, which emphasizes the importance of timely interventions and robust treatment strategies. The recovered population $R(t)$ grows at a faster rate than in the first example, indicating that a significant portion of infected individuals eventually recover and gain temporary immunity, though waning immunity ($\theta = 0.02$) ensures a continuous flow back into the susceptible pool. The vaccinated population $V(t)$ also increases sharply at first, driven by a high vaccination rate ($\gamma = 0.1$), but gradually declines over time due to immunity loss ($\varepsilon = 0.003$). These dynamics collectively underline the importance of maintaining consistent vaccination efforts and integrating strategies that account for immunity waning to achieve sustainable control of anthrax outbreaks in animal populations.

5.2 Real world validation

In this subsection, we validate the performance and applicability of the proposed Genocchi-QLM numerical framework by comparing the simulated results of the anthrax transmission model

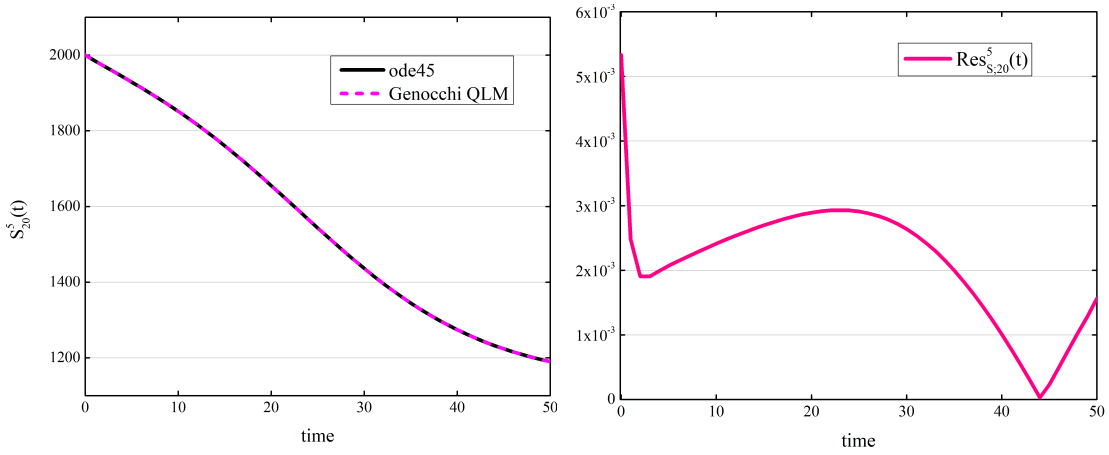

(a) $S^5_{20}(t)$ and `ode45` (b) $Res^5_{S,20}(t)$

Figure 7: The approximate and `ode45` solutions of $S(t)$ for $Q = 20$ (7a) and the residual error (7b) for $\psi = 5$ in Example 2.

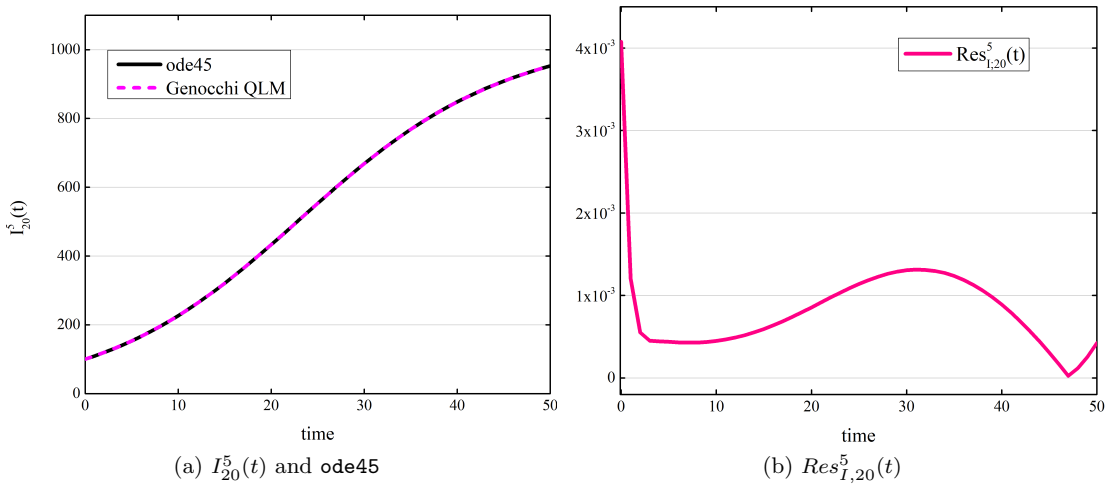

(a) $I^5_{20}(t)$ and `ode45` (b) $Res^5_{I,20}(t)$

Figure 8: The approximate and `ode45` solutions of $I(t)$ for $Q = 20$ (8a) and the residual error (8b) for $\psi = 5$ in Example 2.

with real-world outbreak data. Figure 11 presents the reported number of anthrax cases and corresponding fatalities collected from official epidemiological surveillance data spanning multiple outbreak years form Minnesota and Kazakhstan [19]. These records, gathered from veterinary and public health databases, reflect the dynamics of anthrax outbreaks in animal populations under natural transmission conditions. To replicate the observed trends, we performed numerical simulations of the nonlinear four-compartment model over the time interval using the Genocchi-

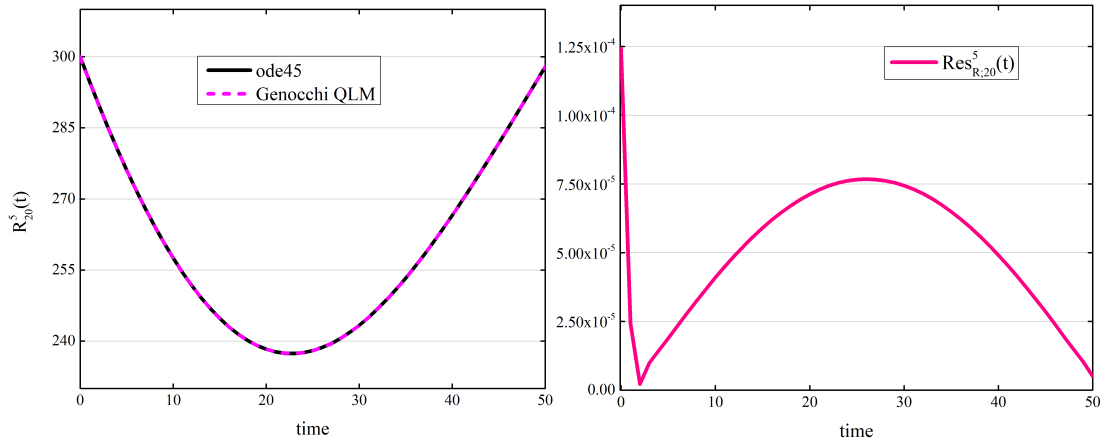

(a) $R^5_{20}(t)$ and `ode45` (b) $Res^5_{R,20}(t)$

Figure 9: The approximate and `ode45` solutions of $R(t)$ for $Q = 20$ (9a) and the residual error (9b) for $\psi = 5$ in Example 2.

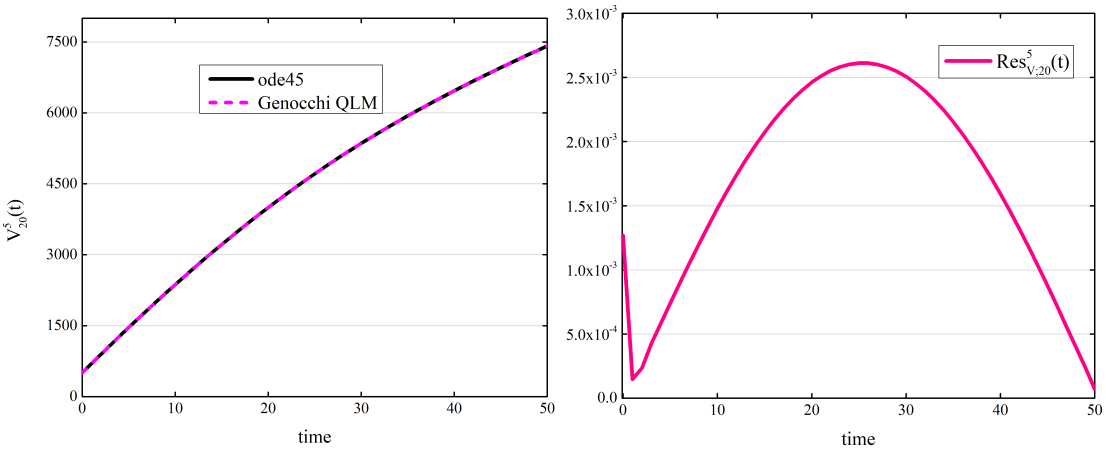

(a) $V^5_{20}(t)$ and `ode45` (b) $Res^5_{V,20}(t)$

Figure 10: The approximate and `ode45` solutions of $V(t)$ for $Q = 20$ (10a) and the residual error (10b) for $\psi = 5$ in Example 2.

QLM method with parameters both reported in the examples. As seen in Figure 11, there is a clear agreement between the simulated dynamics of the infected cases $I(t)$ and the actual case data. The model accurately reproduces the initial rapid rise in the number of infected cases during the early phases of each outbreak, followed by a gradual stabilization or decline due to recovery, mortality, and intervention measures such as vaccination campaigns and quarantine protocols. The validation results in Figure 11 highlight the practical applicability of the developed model

and numerical scheme. This level of agreement reinforces the potential of the Genocchi-QLM method to support decision-making in disease surveillance, risk assessment, and the design of effective intervention strategies in endemic regions [19].

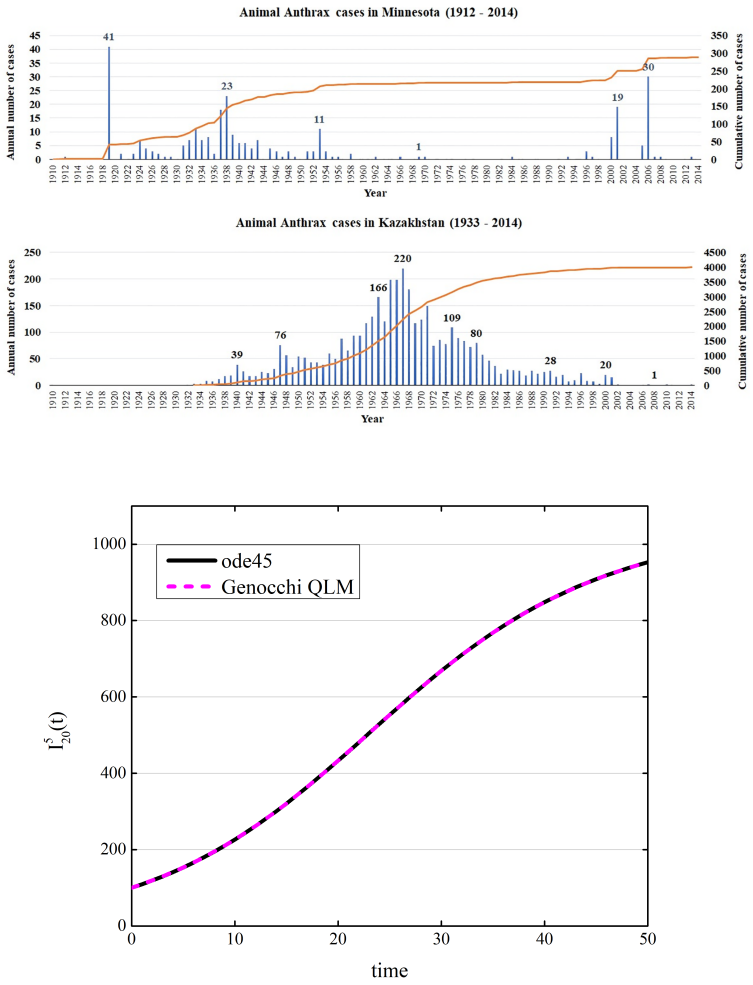

Figure 11: Comparison between the real-world outbreak data in Minnesota and Kazakhstan [19] and the simulated anthrax transmission dynamics obtained using the Genocchi-QLM method.

6 Conclusion

In this study, we developed and analyzed a nonlinear four-compartment anthrax transmission model that captures the interactions between susceptible, infected, recovered, and vaccinated animal populations. The Genocchi-QLM was introduced as a numerical approach, offering high accuracy, stability, and rapid convergence when compared with the classical `ode45` solver. The integration of shifted Genocchi polynomials with the quasilinearization technique allowed the construction of an efficient and scalable numerical framework, further validated through comprehensive error and convergence analyses. The validation of the proposed model against real-world anthrax outbreak data is discussed. The close agreement between the simulated results and empirical observations demonstrates the model's ability to reliably capture the transmission and control dynamics of anthrax in animal populations. This validation confirms that the proposed approach is not only mathematically sound but also practically relevant for epidemiological analysis. Looking forward, the Genocchi-QLM framework can be extended to incorporate fractional-order dynamics to account for memory effects, stochastic formulations to capture variability in transmission and recovery, and integration with larger datasets for predictive modeling and real-time risk assessment.

Acknowledgements

The authors would like to convey their thanks to the Editor and Reviewers for the helpful comments and suggestions which improved the work.

Funding

This research received no external funding.

Conflicts of Interest

The authors declare no conflicts of interest.

References

[1] Ahmed, S., Jahan, S. and Nisar, K.S. *Hybrid Fibonacci wavelet method to solve fractional-order logistic growth model,* Math. Methods Appl. Sci., 46 (2023), 16218–16231.

[2] Alfwzan, W.F., Abuasbe, K., Raza, A., Rafiq, M., Awadalla, M. and Almulla, M.A. *A non-standard computational method for stochastic anthrax epidemic model,* AIP Adv., 2023, 13.

[3] Bylaiah, S., Shedole, S., Suresh, K.P., Gowda, L., Shivananda, B., Shivamallu, C. and Patil, S.S. *Disease prediction model to assess the impact of changes in precipitation level on the risk of anthrax infectiousness among the livestock hosts in Karnataka,* India, Int. J. Spec. Educ, 37 (2022), 711–727.

[4] Chen, X., Bahl, P., de Silva, C., Heslop, D., Doolan, C., Lim, S. and MacIntyre, C.R. *Systematic review and evaluation of mathematical attack models of human inhalational anthrax for supporting public health decision making and response,* Prehosp. Disaster Med., 35 (2020), 412–419.

[5] Croicu, A.M. *An optimal control model to reduce and eradicate anthrax disease in herbivorous animals,* Bull. Math. Biol., 81 (2019), 235–255.

[6] De Vos, V. and Bryden, H. *Anthrax in the Kruger National Park: temporal and spatial patterns of disease occurrence,* Salisbury Med. Bull., 87 (1996), 26–30.

[7] Dragon, D. and Elkin, B. *An overview of early anthrax outbreaks in northern Canada: Field reports of the Health of Animals Branch, Agriculture Canada, 1962–71*, Arctic, 54 (2001), 32–40.

[8] Ebrahimzadeh, A. and Hashemizadeh, E. *Optimal control of non-linear volterra integral equations with weakly singular Kernels based on Genocchi polynomials and collocation method,* J. Nonlinear Math. Phys., 30, (2023) 1758–1773.

[9] Githire, G.T., Kimathi, G. and Wainaina, M. *Analysis of transmission dynamics of anthrax in animals: A modeling approach,* J. Sci. Res. Rep., 23, (2019) 2550127.

[10] Gutting, B., Channel, S., Berger, A., Gearhart, J., Andrews, G., Sherwood, R. and Nichols, T. *Mathematical modelling of transmission dynamics of anthrax in human and animal population,* Microbe, 3 (2008), 78–85.

[11] Harrington, R., Owen-Smith, N., Viljoen, P.C., Biggs, H.C., Mason, D.R. and Funston, P. *Establishing the causes of the roan antelope decline in the Kruger National Park,* South Africa, Biol. Conserv., 90 (1999), 69–78.

[12] Helikumi, M., Lolika, P.O. and Mushayabasa, S. *Implications of seasonal variations, host and vector migration on spatial spread of sleeping sickness: Insights from a mathematical model,* Informatics Med. Unlocked, 24 (2021), 100570.

[13] Idowu, O.K. and Loyinmi, A.C. *Qualitative analysis of the transmission dynamics and optimal control of Covid-19,* Educatum J. Sci. Math. Technol., 10 (2023), 54–70.

[14] Isah, A. and Ibrahim, S. *Shifted Genocchi polynomials operational matrix for solving fractional order system,* Eurasian J. Sci. Eng., 7 (2021), 74–83.

[15] Izadi, M., Ansari, K.J. and Srivastava, H.M. *A highly accurate and efficient Genocchi-based spectral technique applied to singular fractional order boundary value problems,* Math. Methods Appl. Sci., 2024, 48, 905–925.

[16] Izadi, M. and Atangana, A. *Computational analysis of a class of singular nonlinear fractional multi-order heat conduction model of the human head,* Sci. Rep., 14 (2024), 3466.

[17] Izadi, M. and Srivastava, H.M. *Applications of modified Bessel polynomials to solve a nonlinear chaotic fractional-order system in the Financial Market: Domain-splitting collocation techniques,* Computation, 11 (2023), 130.

[18] Izadi, M., Veeresha, P. and Adel, W. *Mathematical and computational analysis of a fractional-order drug abuse model with nonlinear incidence and logistic growth,* Math. Comput. Simul., 240 (2025), 451–472.

[19] Kanankege, K.S.T., Abdrakhmanov, K.S., Alvarez, J., Glaser, L., Bender, J.B., Mukhanbetkaliyev, Y.Y., Korennoy, F.I., Kadyrov, A.S., Abdrakhmanova, A.S. and Perez, A.M. *Comparison of spatiotemporal patterns of historic natural anthrax outbreaks in Minnesota and Kazakhstan,* PLoS One, 14 (2019), e0217144.

[20] Kar, T. and Batabyal, A. *Stability analysis and optimal control of an SIR epidemic model with vaccination,* Biosystems, 104 (2011), 127–135.

[21] Karginov, V.A., Robinson, T.M., Riemenschneider, J., Golding, B., Kennedy, M., Shiloach, J. and Alibek, K. *Treatment of anthrax infection with combination of ciprofloxacin and*

antibodies to protective antigen of Bacillus anthracis, FEMS Immunol. Med. Microbiol., 40 (2004), 71–74.

[22] Lembo, T., Hampson, K., Auty, H., Beesley, C.A., Bessell, P., Packer, C., Halliday, J., Fyumagwa, R., Hoare, R., Ernest, E., Mentzel, C., Mlengeya, T., Stamey, K., Wilkins, P.P. and Cleaveland, S. *Serologic surveillance of anthrax in the serengeti ecosystem, Tanzania, 1996-2009,* Emerg. Infect. Dis., 17 (2011), 387–394.

[23] Mackey, C. and Kribs, C. *Can scavengers save zebras from anthrax? A modeling study,* Infect. Dis. Model., 6 (2021), 56–74.

[24] Mushayabasa, S. *Global stability of an anthrax model with environmental decontamination and time delay,* Discrete Dyn. Nat. Soc., 2015 (2015), 573146.

[25] Mushayabasa, S., Marijani, T. and Masocha, M. *Dynamical analysis and control strategies in modeling anthrax,* Comput. Appl. Math., 36 (2017), 1333–1348.

[26] Mwakapeje, E.R., Høgset, S., Fyumagwa, R., Nonga, H.E., Mdegela, R.H. and Skjerve, E. *Anthrax outbreaks in the humans-livestock and wildlife interface areas of Northern Tanzania: a retrospective record review, 2006–2016,* BMC Public Health, 18 (2018), 106.

[27] Oh, S.Y., Chateau, A., Tomatsidou, A., Elli, D., Gula, H., Schneewind, O. and Missiakas, D. *Modeling gastrointestinal anthrax disease* Res. Microbiol., 174 (2023), 104026.

[28] Osman, S., Makinde, O.D. and Theuri, D.M. *Mathematical modelling of transmission dynamics of anthrax in human and animal population,* Math. Theory Model., 8 (2018) 47–67.

[29] Pantha, B., Day, J. and Lenhart, S. *Optimal control applied in an anthrax epizootic model,* J. Biol. Syst., 24 (2016), 495–517.

[30] Raymond, B., Wyres, K.L., Sheppard, S.K., Ellis, R.J., Bonsall, M.B. and Guttman, D.S. *Environmental factors determining the epidemiology and population genetic structure of the Bacillus cereus group in the field,* PLoS Pathog., 6 (2010), e1000905.

[31] Raza, A. and Abdella, K. *Analysis of the dynamics of anthrax epidemic model with delay,* Discover Appl. Sci., 6 (2024), 128.

[32] Saad-Roy, C.M., van den Driessche, P. and Yakubu, A-A. *A mathematical model of anthrax transmission in animal populations,* Bull. Math. Biol., 79 (2016), 303–324.

[33] Sabir, Z. and Simbawa, E.*A machine learning computational approach for the mathematical anthrax disease system in animals,* PLoS One, 20 (2025), e0320327.

[34] Savransky, V., Ionin, B. and Reece, J. *Current status and trends in prophylaxis and management of anthrax disease,* Pathogens, 9 (2020), 370.

[35] Stella, E., Mari, L., Gabrieli, J., Barbante, C. and Bertuzzo, E. *Permafrost dynamics and the risk of anthrax transmission: A modelling study,* Sci. Rep., 10 (2020), 16460.

[36] Turner, W.C., Imologhome, P., Havarua, Z., Kaaya, G.P., Mfune, E., Mpofu, I.D.T. and Getz, W.M. *Soil ingestion, nutrition and the seasonality of anthrax in herbivores of Etosha National Park,* Ecosphere, 4 (2013), 1–19.

[37] Van den Driessche, P. *Reproduction numbers of infectious disease models,* Infect. Dis. Model., 2 (2017), 288–303.

[38] Yüzbaşı, Ş. and Izadi, M. *Bessel-quasilinearization technique to solve the fractional-order HIV-1 infection of CD4+ T-cells considering the impact of antiviral drug treatment,* Appl. Math. Comput., 431 (2022), 127319.